Available online at www.sciencedirect.com
SCIENCE DIRECT
Journal of Catalysis 226 (2004) 351–362
JOURNAL OF CATALYSIS
www.elsevier.com/locate/jcat

Synthesis of uniform diameter single wall carbon nanotubes in Co-MCM-41: effects of CO pressure and reaction time

Yuan Chen, Dragos Ciuparu, Sangyun Lim, Yanhui Yang, Gary L. Haller, Lisa Pfefferle *

Department of Chemical Engineering, Yale University, New Haven, CT 06520, USA

Received 9 March 2004; revised 24 May 2004; accepted 2 June 2004

Available online 8 July 2004

Abstract

The influence of the CO pressure and of the duration of catalyst exposure to CO was systematically investigated with respect to the carbon yield, selectivity, and diameter uniformity of single wall carbon nanotubes (SWNT) produced by CO disproportionation over Co-MCM-41 catalysts. The SWNT were characterized by Raman and near infrared (NIR) spectroscopy, while the state of the catalyst and the size of the metallic cobalt clusters were investigated by X-ray absorption spectroscopy (XAS). The experimental results suggest that both the selectivity to SWNT and the uniformity of their diameters are controlled by the relative rates of the following competing processes: cobalt reduction, nucleation of cobalt into clusters, and SWNT growth. It was found that reaction at low CO pressures leads to a wider distribution of diameters and lower SWNT selectivity. The duration of catalyst exposure to CO was found to strongly affect the SWNT selectivity at the early stages of SWNT growth, while it has a minor effect on the SWNT diameter uniformity.

Keywords: Single wall carbon nanotubes; Cobalt clusters; CO pressure; Reaction time

1. Introduction

Incorporation of single wall carbon nanotubes (SWNT) in electronic devices requires materials of uniform electronic properties. Because the electronic properties of the carbon nanotubes depend on their *n* and *m* vectors [1], thus on diameter and chirality, SWNT synthesis methods producing a narrow diameter distribution are highly desirable. We have shown that SWNT can be produced by CO disproportionation on a cobalt catalyst incorporated by isomorphous substitution of silicon in the pore walls of the MCM-41 mesoporous molecular sieve [2]. We have also shown that the diameter of SWNT produced with this catalytic system can be engineered by controlling the size of the metallic Co clusters that initiate the growth of the SWNT [3].

Several studies have been dedicated to the investigation of the effects of the SWNT synthesis process variables on the overall process performance [4–21]. Many of these studies have reported various effects of the reaction time and pressure on the purity, diameter control, and uniformity of the SWNT produced. The differences in the observed effects are mainly due to the use of different processes [4–6], carbon sources [7–10], or catalytic systems [11–15] for the growth of SWNT. For the Co–Mo catalytic system, which is somewhat similar to our Co-MCM-41 catalyst, the carbon yield and SWNT selectivity increased when the catalyst was exposed to CO for longer than 2 h [15,16].

In our prior investigations we observed that the diameter uniformity of the SWNT produced using this synthesis technique is strongly influenced by the catalyst pretreatment conditions (i.e., prereduction temperature) and CO disproportionation conditions such as the reaction temperature, pressure, and duration. In a recent paper we reported the effects of the template prereduction temperature and CO disproportionation temperature on the diameter uniformity of the nanotubes produced [22]. We have shown that the diameter distribution and quality of SWNT grown in Co-MCM-41 can be engineered by controlling the hydrogen prereduction and reaction temperatures, and that the cobalt incorporated in the MCM-41 matrix becomes more selective to SWNT after partial reduction by hydrogen, while the catalysts that were excessively reduced prior to exposure to CO became less selective for SWNT, producing more amorphous car-

* Corresponding author.
E-mail address: dragos.ciuparu@yale.edu (L. Pfefferle).

0021-9517/$ – see front matter
doi:10.1016/j.jcat.2004.06.006

bon and/or graphite. We have also demonstrated that uniform SWNT diameter (±0.05 nm) can be achieved by using optimized prereduction and reaction temperatures, and that control of cobalt cluster sizes in Co-MCM-41 is the key to SWNT diameter control [22].

In the present contribution we report our investigations on the effects of the growth time and CO pressure during SWNT growth on the diameter uniformity and the quality of the SWNTs produced as qualitatively determined from Raman and near-infrared spectroscopy.

2. Experimental

The Co-MCM-41 catalyst with a 1.00 wt% Co loading and a pore diameter of 2.85 ± 0.1 nm was synthesized using the $C_{16}H_{33}$ $(CH_3)_2NBr$ alkyl template following the procedure described elsewhere [2]. The purity of the silica source affected the reducibility of the cobalt ions in the framework. The catalysts employed in these studies were synthesized using the highly pure Cab-O-Sil silica. Approximately 200 mg of fresh catalysts was loaded into a quartz reactor placed in an electric furnace with very good temperature control for the entire length of the catalyst bed. Prior to exposure to pure CO the catalyst was heated in flowing hydrogen (1 atm) at 20 °C/min from room temperature to 500 °C and reduced isothermally for 30 min. After this prereduction treatment, the catalyst was purged with ultrahigh-purity argon at 500 °C and then heated to 800 °C at 20 °C/min in flowing argon (4 atm). SWNT were grown for 5–120 min at 800 °C under different CO partial pressures ranging from 2 to 6 atm.

The carbon yields were determined from the thermogravimetrical analysis performed in a Setaram SetSys 1750 instrument using a holey crucible that prevents mass-transfer limitations. The weight of the sample was monitored during two consecutive temperature programs for each sample, the second being used as a baseline for the first.

Raman spectra were recorded with as-synthesized SWNT samples, without any purification or pretreatment, on a LabRam instrument from Jobin Yvon Horiba equipped with an Olympus confocal microscope (at 532 nm excitation wavelength). Integration times were around 15 s for each spectrum, and each spectrum was the average of five scans. Multiexcitation wavelength Raman spectra were collected at the University of Connecticut with a Renishaw Ramanscope in the backscattering configuration under the same experimental conditions with different integration times. The spectra were obtained using four different lasers with wavelengths of 488 nm (2.54 eV), 514.5 nm (2.41 eV), 633 nm (1.96 eV), and 785 nm (1.58 eV).

Absorption spectra in the near-infrared (NIR) region were recorded for SWNT samples dispersed by sonication in *N*,*N*-dimethylformamide (DMF) using a Nicolet NEXUS Fourier transform infrared spectrometer equipped with a quartz beam splitter.

Diameter distribution was also probed by high-resolution transmission electron microscopy (HR-TEM). Micrographs were obtained on a Tecnai F20 (200 kV) microscope from Phillips.

The state of the cobalt catalyst and assessment of the cobalt cluster sizes were determined from the X-ray absorption spectra collected at the beam line X23A2 of the National Synchrotron Light Source at Brookhaven National Laboratory. Analysis of the X-ray absorption spectra was performed following the procedures described in detail in our previous work [22].

3. Results and discussion

Two series of experiments were designed to investigate the influence of the CO pressure and the duration of nanotube growth on the overall carbon yield, and the selectivity and diameter uniformity of the SWNT produced. Catalyst samples removed from the reactor after SWNT growth under different conditions, without any purification or pretreatment, were studied by extended X-ray absorption fine structure (EXAFS) spectroscopy to determine the cobalt oxidation state and the size of the cobalt clusters in the catalysts after reaction. These results were further correlated with the carbon yield and SWNT selectivity determined from the complementary thermo-gravimetrical analysis, and Raman and NIR spectroscopy in order to understand the mechanism by which the CO pressure and growth duration influence the SWNT synthesis performance. The effect of each investigated process variable is discussed in separate sections below.

3.1. Carbon monoxide pressure

For the first series of experiments catalyst samples pretreated in pure hydrogen at 500 °C for 30 min were exposed to pure CO for 60 min at 800 °C under different CO pressures ranging from 2 to 6 atm.

The Raman spectra recorded with the catalyst after SWNT growth under different CO pressures are given in Fig. 1. Each spectrum is the average of five spectra recorded at different locations in the same sample. Three types of spectral features are observed in each spectrum: the peaks in the Raman breathing mode (RBM) region ($\tilde{\nu} \leqslant 350$ cm^{-1}), characteristic for SWNT, provide information about tube diameters [23,24] and chirality [25,26]; the D band at approximately 1300 cm^{-1} is assigned to disordered and/or defective carbon species; and the peak complex around 1600 cm^{-1}, known as the G band, is characteristic of ordered carbon species such as carbon nanotubes and graphite.

The Raman spectrum of the SWNT grown at 2 atm shows several peaks in the RBM region, suggesting that the diameters of the nanotubes produced at this reaction pressure have a wide distribution. The intensity of the lower frequency RBM peaks, corresponding to SWNT of larger diameters,

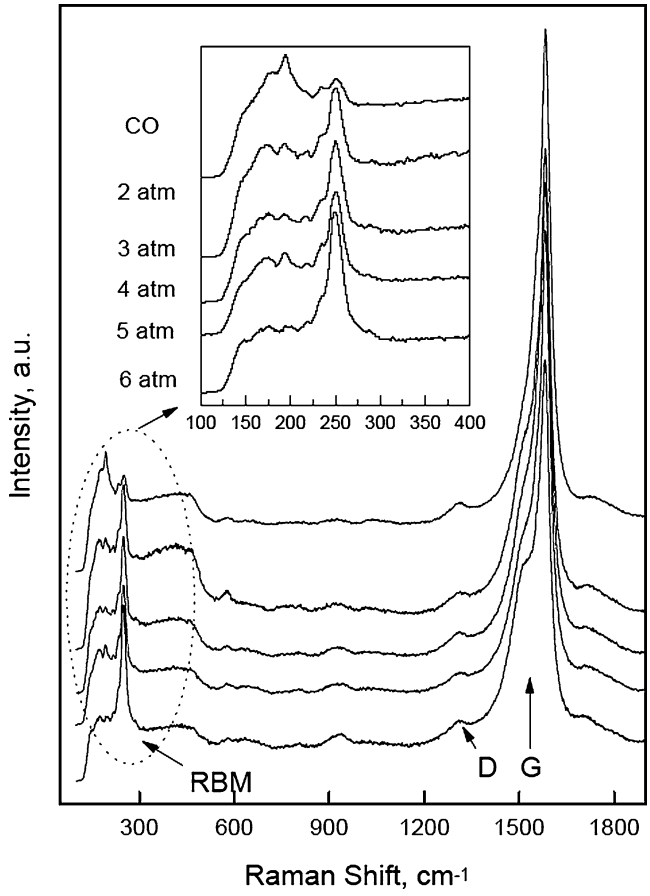

Fig. 1. Raman spectra recorded for SWNT grown at different CO pressures. The inset shows an enlargement of the Raman breathing mode region.

decreases as the CO pressure increases. The RBM region of the spectrum recorded with the SWNT grown at 6 atm shows a single, strong peak, indicative of a narrow diameter distribution of the SWNT produced. The presence of a narrow distribution of tube diameters in the SWNT sample grown at 6 atm has been confirmed by multiexcitation wavelength Raman spectroscopy as depicted in Fig. 2a. In contrast with the spectra recorded for the sample synthesized at 2 atm CO given in Fig. 2b, the spectra for the high-pressure sample show only one peak for each laser frequency. It should be noted that the laser frequencies at 633 nm (1.96 eV) and 785 nm (1.58 eV) are more sensitive to the larger tubes in the samples grown at 2 atm CO than the higher energy lasers. The intensity of the RBM peaks relative to the intensity of the G band determined from the multiple excitation Raman spectra increased when the reaction pressure increased. The total carbon loading determined by TGA and plotted as a function of pressure in Fig. 3 also shows an increasing trend as the CO pressure increases. These results indicate a strong effect of the CO pressure on both carbon yield and selectivity for SWNT, and diameter uniformity. At higher CO pressures larger amounts of carbon deposit on the surface in the form of SWNT of a narrower diameter distribution. These results are consistent with previous experimental observations of Nikolaev et al. for SWNT synthesis by thermal decomposition of iron pentacarbonyl in a heated flow of carbon monoxide [12].

Because of their weak intensity and the strong dependence of resonances on the tube diameter [27,28], the relative peak intensities for the several peaks in the RBM region

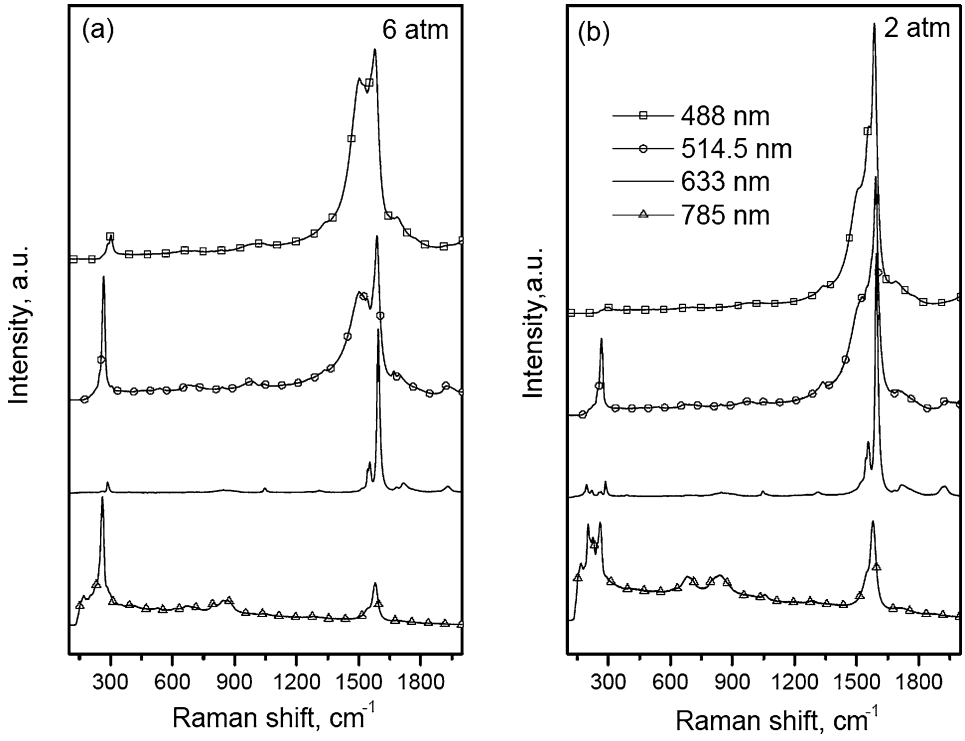

Fig. 2. Multiexcitation wavelength Raman spectra recorded for SWNT grown at 6 (a) and 2 atm CO pressure (b).

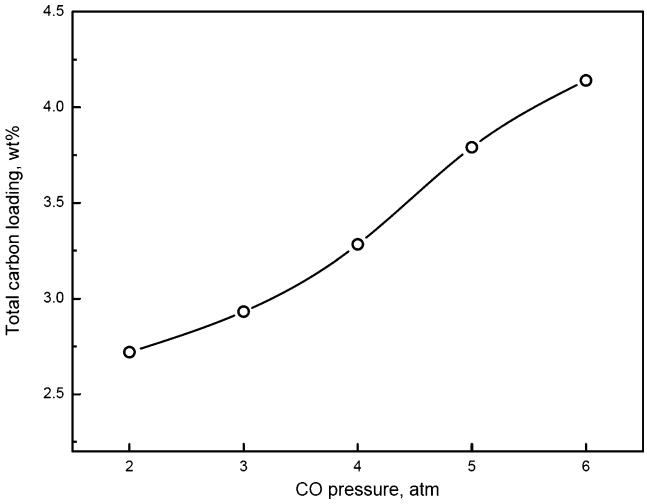

Fig. 3. Total carbon yield as a function of the CO pressure.

cannot be easily related to the abundance of each tube diameter in the sample. Optical spectroscopy of the SWNT produced at different pressures provides a more sensitive diagnostic technique for analyzing the relative concentrations of tubes of different diameters in our samples.

The electronic structure of the SWNT can be easily altered by adsorption of chemical species on their surface [29]. To minimize such processes and preserve their original electronic structure we dispersed the SWNT samples, without purification or any other treatment, in dimethylformamide by sonication for 5 min. The DMF solvent was preferred because of its wide transmission window, and because it was reported to require a minimal application of ultrasound to disperse the SWNT [30].

The NIR absorption spectra in Fig. 4a recorded for nanotubes grown at different CO pressures show the main characteristic absorption band centered at approximately 1200 nm. This band can be assigned to the electronic transitions between the first pair or the second pair of van Hove singularities (VHS), depending on the diameter of the SWNT in the sample. According to the SWNT electronic band theory [31], if the band at 1200 nm comes from the second VHS, the diameter of the SWNT should be around 2–3 nm, while if it belongs to the first VHS, the diameter is about 1 nm. From the Raman spectra and the TEM results we can only identify SWNT with diameters below 1 nm, therefore this band is assigned to the first VHS, i.e., E_{11}^{S}.

Optical spectroscopy has been previously employed to perform analysis of the SWNT mean diameter and diameter distribution in carbon nanotube samples [32]. Aggregation of nanotubes into bundles substantially broadens and redshifts the absorption features [33,34]. Akasaka et al. used a three-step wet chemistry procedure to purify and separate the SWNT, and observed fine structures in the optical absorption spectra of the carbon nanotube samples, which were assigned to SWNT with different diameters and helicity [35]. The short-time sonication performed in our sample preparation procedure does not isolate the SWNT from bundles, as suggested by the broad spectra shown in Fig. 4a and confirmed by many TEM experiments. However, the rela-

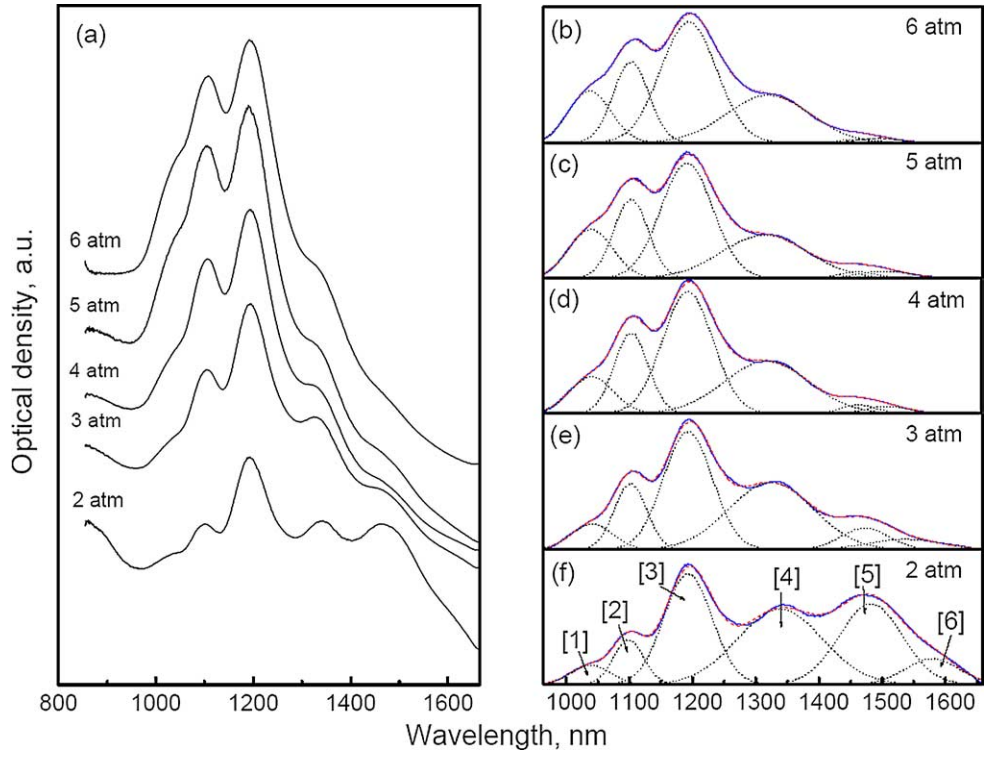

Fig. 4. NIR spectra of SWNT dispersed in DMF: (a) Spectra of SWNT synthesized at different CO pressures from 2 to 6 atm; (b–f) spectra after background correction (solid lines), and the six peaks resulting from deconvolution using a Gaussian-fitting function (dot lines).

tive differences in the diameter of these SWNT samples are clearly evidenced in these spectra. The solid lines in Figs. 4b to 4f show the baseline-corrected NIR absorption spectra in the range of 960–1660 nm for SWNT samples grown at different pressures. These spectra were deconvoluted into six peaks identified and resolved in our spectra using a Gaussian fitting function. As discussed above, because our tubes are most likely bundled, the peaks resulting from deconvolution correspond to the average electronic properties of SWNT in bundles. Weisman et al. pointed out that the tight-binding model badly underestimated the apparent scattering arising from chiral variation at a given diameter [36]. Using the empirical Kataura plot developed by these authors we assigned the six peaks to six groups of bundled SWNT having average diameters from 0.68 to 1.38 nm. Groups 1 and 2 have smaller diameters than groups 5 and 6, while SWNT with absorptions in groups 3 and 4 have intermediate diameters and are the major species produced in each sample.

Assuming the SWNT synthesized in Co-MCM-41 show the normal 1:2 distribution between metallic and semiconducting tubes [1], respectively, the narrow diameter distribution suggested for the semiconducting tubes in the NIR spectroscopy was verified in the multiple excitation wavelength Raman spectroscopy experiment, which shows a single peak at each laser line for the samples grown at high CO pressure. Therefore, the diameter distribution of the semiconducting SWNT determined here from optical spectroscopy is representative for the overall diameter distribution of the SWNT sample, including the metallic tubes. Plotting the normalized area of each peak resulting from deconvolution in Fig. 5a for samples grown at different pressures we observed that the fraction of smaller diameter tubes in groups 1 and 2 increased when the CO pressure increased, while the fraction of larger diameter tubes in groups 5 and 6 decreased with the increase in CO pressure, as depicted in Fig. 5b. Therefore it is concluded that higher CO pressure produces smaller diameter SWNT while lower CO pressure produces larger diameter SWNT.

We have previously demonstrated that the isomorphous substitution of Si ions in the MCM-41 by cobalt ions impedes the complete reduction of cobalt to metal under moderate reduction conditions, i.e., treatment at 500 °C in pure hydrogen [3]. A direct consequence of this stabilization effect of the MCM-41 framework on the Co^{2+} ions is that exposure of a catalyst pretreated in hydrogen at 500 °C to pure CO at SWNT synthesis temperatures leads to the formation of very small metallic cobalt clusters in the MCM-41 molecular sieve. We have demonstrated that these cobalt clusters control the diameter of SWNT grown [3]. Along these lines, the diameter distribution of the SWNT provides indirect information on the size distribution of the cobalt clusters formed during SWNT synthesis. The signatures of the large SWNT observed in the Raman spectra in Figs. 1 and 2b and in the NIR spectra in Fig. 4a suggest that catalyst exposure to 2 atm CO produces larger cobalt clusters than those produced by exposure to 6 atm CO at the same reaction temperature. On the other hand, the larger number of cobalt clusters presumably formed during reduction at higher CO pressure should provide more sites for SWNT growth and, assuming at least first-order SWNT growth kinetics with respect to the CO concentration, the higher CO pressure should increase the SWNT growth rate. These two rationales are consistent

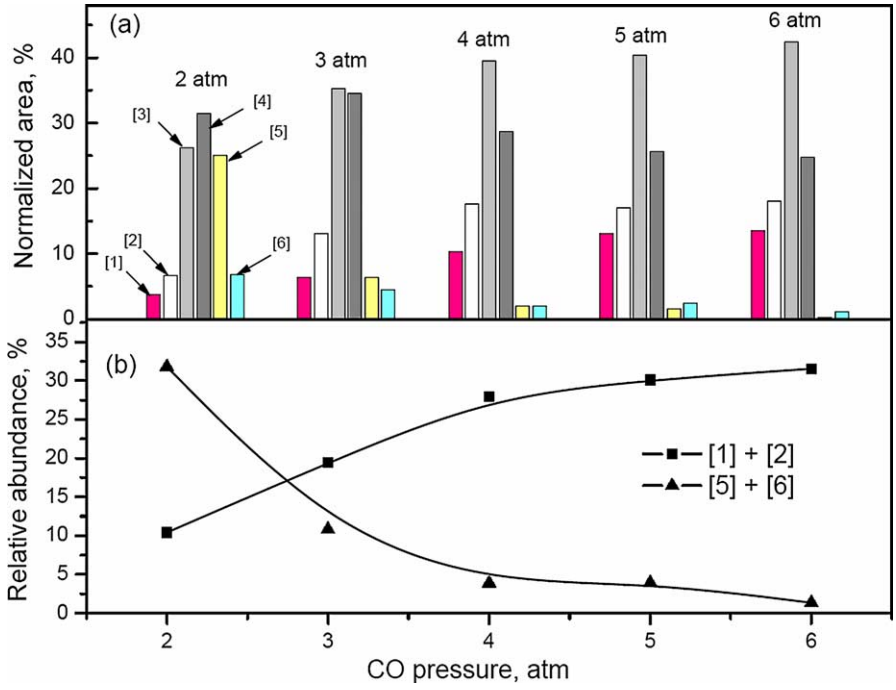

Fig. 5. (a) The size distribution of semiconducting SWNT synthesized at different CO pressures as determined from NIR spectra. (b) The relative abundances of small and large tubes as functions of CO pressure during SWNT synthesis.

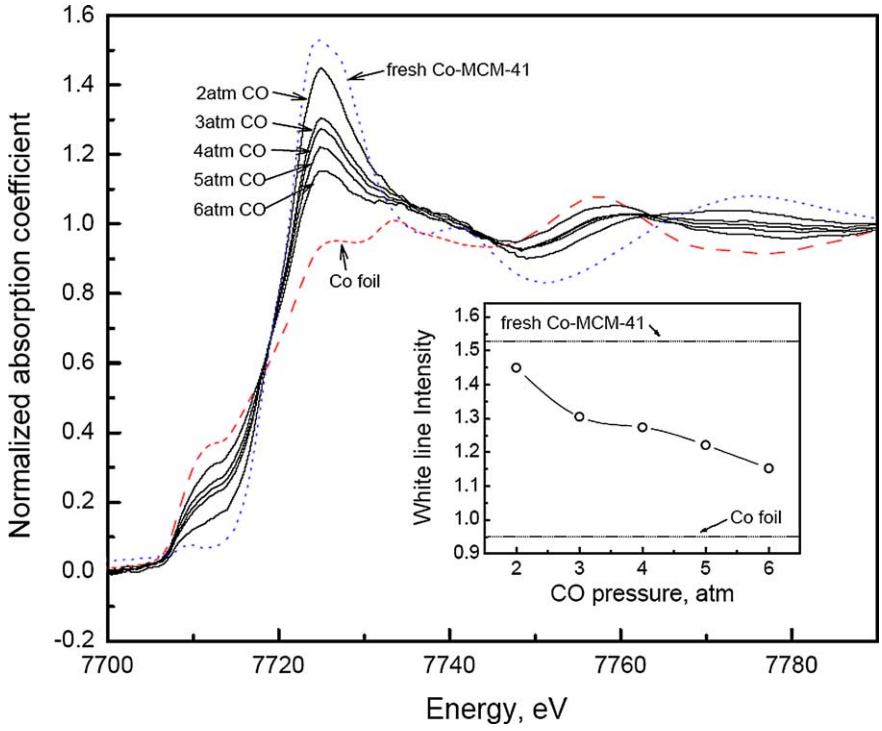

Fig. 6. Normalized EXAFS spectra near Co *K* edge recorded for Co-MCM-41 loaded with carbon after reaction at different CO pressures. Spectra for the fresh Co-MCM-41 and cobalt foil are given as references. The inset shows the correlation between the intensity of the white line and the CO pressure.

with the increase in the carbon yield when the CO pressure increases, as observed in Fig. 3. It should be noted that the intensity of the RBM peak relative to the intensity of the G band for all 4 laser frequencies also increases as the pressure increases, suggesting that more graphitic carbon is formed at lower pressures. Since we have shown that small particles are selective for SWNT growth and large particles form predominantly graphite [22], this evolution is a second reason to propose that exposure at lower CO pressures leads to the formation of larger cobalt particles.

These observations are intriguing as, assuming a non-zero positive order for the kinetics of cobalt reduction with respect to CO, one would expect a higher CO partial pressure to accelerate Co reduction, generate a higher metallic cobalt concentration on the pore wall surface, and, thus, form larger metallic clusters. Quantitative determinations of the cobalt cluster sizes after reaction at different pressures are thus required to understand these intriguing experimental results. The state of cobalt and the size of the metallic clusters in the catalyst samples were investigated by EXAFS. The white line features and the preedge peak details near the Co *K* edge (7709 eV) were obtained after energy edge calibration using a cobalt foil reference, background removal, and edge-step normalization using the FEFFIT program [37], following a procedure described elsewhere [22]. The resulting spectra for samples reacted at different pressures are shown in Fig. 6, along with the spectra for the fresh, fully oxidized catalyst and that of the cobalt foil, given as references.

The near-edge region of the X-ray absorption spectra recorded for the cobalt foil shows a strong preedge peak characteristic of metallic cobalt. The white line feature resulting from the density of unoccupied states above the Fermi level is attributed to the oxidized cobalt. The increase of the preedge spectral feature for the Co-MCM-41 catalyst after SWNT growth, associated with the decrease in the white line intensity (the white line peak height) as the CO pressure increased, is direct evidence for the increase in the amount of completely reduced cobalt in the catalyst as the SWNT are synthesized at higher CO pressure. The inset in Fig. 6 shows the variation of the intensity of the white line with the CO pressure, indicative of the degree of cobalt reduction in the catalyst. While some of the cobalt reduced during reaction may be reoxidized after catalyst exposure to the atmosphere leading to the increase of the white line intensity, the strong intensity of the preedge feature suggests that the concentration of the reoxidized cobalt is small and should not affect the overall trend of the variation of the white line intensity with the CO pressure. The spectra of the fresh Co-MCM-41 and of the Co foil have white line intensities of 1.53 and 0.95, respectively. As the CO pressure increases from 2 to 6 atm, the intensity of the white lines decrease from 1.44 to 1.15, clearly showing different degrees of cobalt reduction for reaction at different CO pressures. The intermediate intensity of white line and the position of the preedge peaks for the Co-MCM-41 samples after SWNT growth indicate that Co in MCM-41 is a mixture of metallic Co clusters and oxidized cobalt isomorphously substituted for Si^{4+} in the MCM-41 framework.

The FEFFIT program was employed to fit the EXAFS spectra using the first shell for both reduced and oxidized

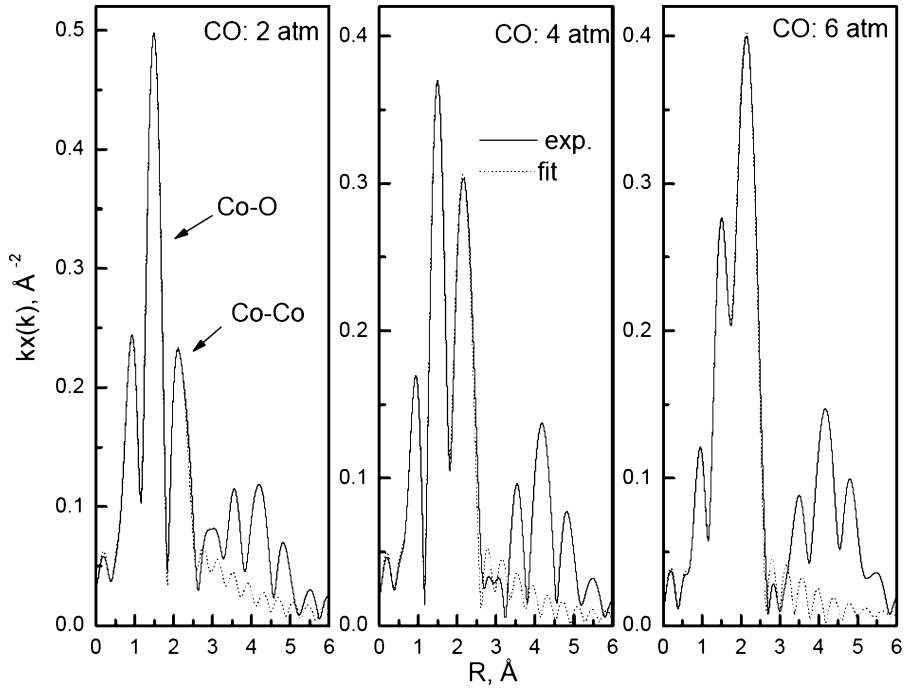

Fig. 7. EXAFS data for Co-MCM-41 catalysts after reaction at different CO pressures in R space along with the fittings of the spectra with theoretical models.

cobalt species (Co and Co_3O_4), as generated by the FEFF6 program [38]. In a previous study we observed that there was no significant contribution of the Co–C interaction to the fitting results for the spectra collected for catalyst samples reacted with CO under the conditions used in this study [39]. The fitting was limited to a k range from 2.2 to 10.0 Å^{-1}, k weight, with modified Hanning window, $dk = 1.0$ Å^{-1}, and an R range from 1.2 to 2.7 Å. The energy shifts for each shell varied insignificantly for samples reacted under different CO pressures; therefore the energy shift was set constant at 5.57 eV for the Co–Co shells and 2.41 eV for the Co–O shells, respectively. The passive electron reduction factor (S_0^2) was set to 0.9, as recommended by Rehr and co-workers [40]. Examples of the fitting results are shown in Fig. 7, and the corresponding Co–Co and Co–O first-shell coordination numbers are given in Table 1.

The k-weighted EXAFS spectra and the fitting results for samples reacted under 2, 4, and 6 atm CO pressure given in Fig. 7 show good agreement between the fittings and the experimental data in the selected fitting window. The fitting results were not highly sensitive to the windowing parameters. As expected, the two major peaks corresponding to the Co–O and Co–Co bonds show that the concentration of reduced cobalt increases with the CO pressure.

The changes in the structural parameters resulting from the fitting and presented in Table 1 confirm the different degrees of Co reduction suggested by the evolution of the white line intensity and the preedge peaks in Fig. 6. The Co–O coordination number decreases when CO pressure increases.

The X-ray absorption spectroscopy has been used previously to determine the size of nanoparticles because of the strong and nonlinear correlation between the particle diameter and the coordination number of atoms in clusters smaller than 2 nm [3,41,42]. However, application of EXAFS to determine the size of finely dispersed clusters is limited by the insensitivity of this technique to polydispersity [43,44]. While in our previous EXAFS studies of SWNT growth on Co-MCM-41 we noted that the Co cluster size determined from EXAFS analysis averages in the large Co particles outside the pores of the MCM-41 material, the uniform distribution of the diameters of the SWNT produced, and the high selectivity for SWNT led us to conclude that the values predicted from the EXAFS spectra were close to the actual values because the Co particles growing SWNT were fairly uniform in size [3]. The presence of significant amounts of large Co particles should have altered both the SWNT diameter uniformity and the SWNT selectivity by production of graphite and amorphous carbon. Therefore, in these previ-

Table 1
Structure parameters determined from the EXAFS fittings for Co-MCM-41 catalysts reacted at different CO pressures

CO pressure (atm)	Co–O first shell			Co–Co first shell		
	N_{Co-O}[a]	dR (Å)[b]	σ^2[c]	N_{Co-Co}[d]	dR (Å)[b]	σ^2[c]
2	1.87 ± 0.91	0.14 ± 0.02	0.85	2.44 ± 1.92	-0.04 ± 0.05	0.85
3	1.31 ± 0.66	0.13 ± 0.02	0.67	3.95 ± 1.43	-0.03 ± 0.02	0.67
4	1.13 ± 0.55	0.13 ± 0.02	0.75	4.60 ± 1.34	-0.03 ± 0.02	0.75
5	0.93 ± 0.51	0.13 ± 0.02	0.68	4.95 ± 1.17	-0.03 ± 0.01	0.68
6	0.73 ± 0.27	0.13 ± 0.01	1.48	7.10 ± 0.87	-0.02 ± 0.01	0.80

[a] N_{Co-O} average first-shell coordination of cobalt–oxygen.
[b] dR deviation from the effective half-path-length R (R is the interatomic distance for single scattering paths).
[c] σ^2 ($\times 10^{-2}$ Å^2) mean-square deviation in R.
[d] N_{Co-Co} average first-shell coordination of cobalt.

ous high CO pressure studies, there were no contradictions between the EXAFS results and the Raman spectra of the SWNT produced. However, the EXAFS results in this study are in an apparent contradiction with the diameter distributions of the SWNT grown on Co-MCM-41 at different CO pressures as characterized by TEM, and Raman and NIR spectroscopy: after reaction at 6 atm CO the catalyst shows cobalt clusters with larger Co–Co coordination numbers than those observed after reaction at 2 atm CO, but grows SWNT of smaller diameters with uniform distribution. In contrast, metallic clusters with lower Co–Co coordination number observed in the sample reacted at 2 atm CO produced SWNT with larger diameters and a wider diameter distribution.

The starting point in the interpretation of these experimental data is the understanding of the physical and chemical processes taking place in the catalytic system during the SWNT synthesis process. Our previous studies showed that the hydrogen prereduction treatment only partially reduces the cobalt in the catalyst without generating any metallic cobalt clusters [22]. During exposure to pure CO at higher temperature, however, cobalt is gradually completely reduced to metal and becomes more mobile on the surface. The EXAFS spectra plotted in the *R* space in Fig. 7 clearly show that the intensity of the Co–Co peak increases and that of the Co–O decreases as the reaction pressure increases for catalysts prereduced under identical conditions and reacted for the same duration of time at different CO pressures, giving direct evidence that more cobalt is reduced as the catalyst is exposed to higher CO pressures. Whether the cobalt migrates through the silica framework as an ion or a metal atom is not yet understood and the clarification of this mechanism is beyond the scope of this study. However, once the reduced atoms reach the pore wall surface, they start to nucleate into clusters of increasing size before they initiate the growth of a carbon nanotube or of other types of carbon on their surface. Since both the solubility of carbon into metallic particles [45] and the ability of the particle to dissociate CO decrease with the particle size, there is likely a minimum size required for the metallic Co cluster to initiate the growth of a SWNT. Along these lines, under certain reaction conditions, very small cobalt metal clusters that are not active for SWNT growth would likely be present in the pores. It should also be noted that we have observed that the growth of the Co clusters likely ceases once their surface is covered with carbon. Therefore, the final size and the size distribution of the cobalt clusters is controlled by the relative rates of the several physical and chemical processes affecting the structure and the state of the catalyst during the SWNT synthesis: cobalt reduction and migration through the pore wall to the pore wall surface, cobalt nucleation and growth into clusters, and carbon deposition.

With respect to the kinetics of cobalt nucleation and cluster growth, a weak interaction between the cobalt clusters and the pore wall would lead to rapid sintering and formation of large particles. Because in many instances the cobalt clusters formed in our Co-MCM-41 catalysts during SWNT growth are very small (subnanometer), there is likely a strong interaction between the metallic clusters and the pore wall. This strong interaction may be an effect of the radius of curvature; i.e., a smaller pore radius of curvature would cause a stronger interaction between the Co clusters and the pore wall. This effect has been systematically investigated elsewhere [39]. In addition to the pore radius of curvature effect, a chemical-anchoring effect of the Co^{2+} ions still in the silica framework may also stabilize small Co metallic clusters against sintering. Stabilization of small metallic clusters by chemical anchoring has been previously observed in NaY zeolites where Fe^{2+} and Cr^{3+} ions stabilized small Pt clusters against sintering [46]. The same effect has also been reported for rhodium clusters in chromium ion-exchanged NaY zeolites [47]. Although these two effects are hard to demonstrate individually, they may both contribute to the stabilization of small metallic clusters in the MCM-41 molecular sieve.

Taking into account the above mechanisms, it is likely that a multimodal distribution of the Co particle size is responsible for the apparent contradiction between the EXAFS data and the Raman and NIR spectroscopy results, respectively. First, it should be noted that the overall carbon yield is considerably lower at low CO pressure, suggesting that fewer Co species are available for carbon deposition, as confirmed by the X-ray absorption results shown in Fig. 7. Assuming first-order reduction kinetics with respect to CO, a lower surface Co concentration is consistent with a lower degree of Co reduction at lower CO pressure, as suggested by the variations of the white line intensity and the preedge spectral feature depicted in Fig. 6. The Raman spectra suggest that a larger fraction of the carbon is graphite in the sample produced at lower pressure, consistent with the presence of large Co particles. SWNT with a broad distribution of diameters are also observed in the TEM micrograph in Fig. 8A recorded for the sample reacted at 2 atm, while the image in Fig. 8B shows uniform diameter SWNTs in the characteristic closed hexagonal packing [3]. TEM analysis did not give evidence of large Co particles on the surface most likely because there are just a few large particles in one specimen and their size may still be below 2.85 nm, thus still being accommodated inside the pores of the MCM-41 material. These results suggest a small fraction of reduced cobalt can be converted into larger particles at lower CO pressures. Second, the lower Co–Co coordination number can be explained by the presence of many clusters of smaller diameter that counterbalance the contribution of the large diameter particles to the overall Co–Co coordination number observed experimentally. Therefore, the overall picture consistent with these results is an interior pore wall surface decorated with many cobalt clusters with sizes below the minimum size required to grow carbon nanotubes, and a few larger cobalt clusters with a wide distribution of sizes and able to grow SWNT, graphite, and amorphous carbon. The small Co clusters are strongly anchored to the pore wall surface, most likely on Co^{2+} ions embedded into the pore wall near the surface. This

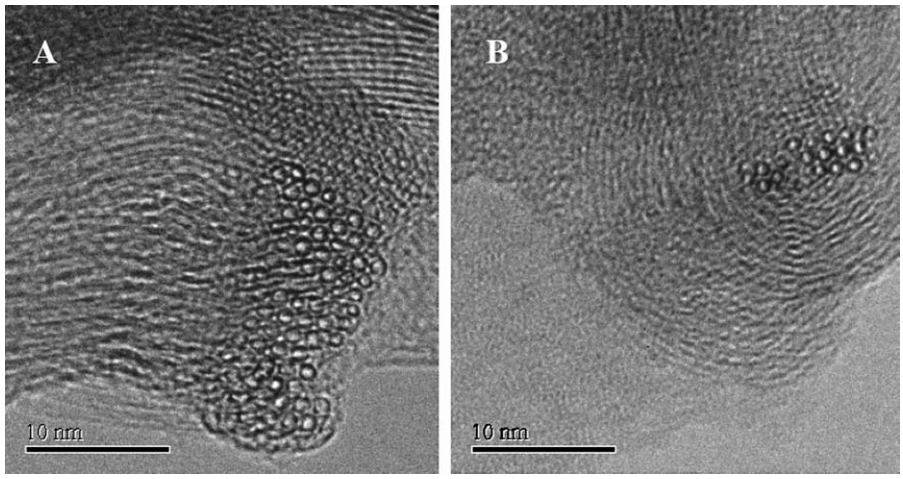

Fig. 8. Transmission electron micrographs showing (A) as-synthesized SWNT of different diameters grown on Co-MCM-41 at 2 atm CO pressure and 800 °C, and (B) as-synthesized uniform diameter SWNT grown at 6 atm CO pressure and 800 °C.

bimodal distribution of Co cluster sizes will result in an average Co–Co coordination number (weighted by the volume of particles of each size, not by their diameter) corresponding to a cluster size somewhere between the diameters of the large and the small Co clusters present in our sample. Depending on the relative concentration of these two populations of clusters/particles, the resulting average size could be closer to the smaller or to the lager particles size. It has been shown from calculations that, for example, a particular bidisperse system containing Pt clusters of 13 and 1415 atoms will show the same Pt–Pt coordination number with a system containing monodisperse clusters formed from 147 Pt atoms [44]. Taking into account the low carbon yield and low Co–Co coordination number observed for the sample reacted at 2 atm CO, it is likely that most of the reduced cobalt in this sample is in the form of cobalt clusters of sizes smaller than the critical size required for carbon growth and/or unreduced Co^{2+}. The presence of few large Co clusters that generate SWNT, graphite, and amorphous carbon is most likely due to the slower rate of carbon growth at lower pressures, thus giving more time to the small clusters to nucleate before they can grow either SWNT or other carbon species. This is also consistent with the low carbon yield and SWNT selectivity at low CO pressures and with the X-ray absorption experiments showing less metallic cobalt evolved after reaction at 2 atm. However, some larger cobalt particles may also be a product of the more rapid reduction of the small concentration of Co^{3+} species ($\sim$ 4% from the total cobalt loading) initially present in the sample. This species reduces at lower temperatures, as discussed elsewhere [39]. This would contribute a larger fraction of the metal clusters in the 2 atm case because the total fraction of reduced cobalt at this pressure is smaller.

3.2. Reaction time

A separate series of experiments was designed to investigate the influence of duration of the catalyst exposure to CO on the SWNT synthesis performance quantified by the yield, selectivity, and diameter uniformity of the nanotubes produced. SWNT were grown by catalyst exposure to CO for different times between 5 and 120 min following the same pretreatment by hydrogen at 500 °C. The reaction conditions were controlled at 800 °C and 6 atm CO pressure. The Raman spectra of the Co-MCM-41 loaded with carbon after exposure to CO for different durations are shown in Fig. 9.

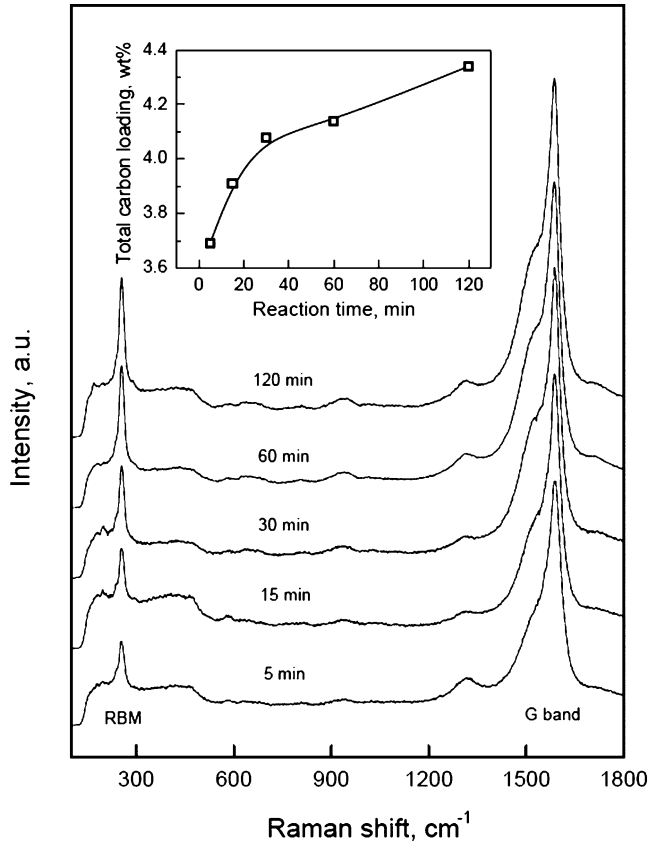

Fig. 9. Raman spectra recorded for SWNT grown at different reaction times. The inset shows the total carbon yield as a function of reaction time.

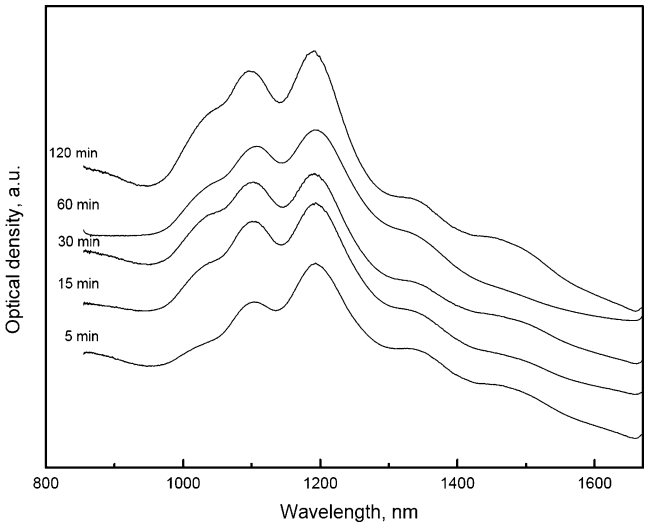

Fig. 10. NIR spectra of SWNT synthesized at different reaction times.

The positions of the peaks in Raman breathing mode region did not show significant changes when the duration of CO exposure increased from 5 to 120 min. Also, all the spectra showed rather weak D bands, indicating small amounts of amorphous carbon. The intensity of the Raman breathing mode peak observed for all four laser lines used have a slightly increasing trend relative to the intensity of the G bands as the catalyst is exposed to CO for a longer time, indicating that the selectivity to SWNT slightly increased. This behavior suggests that both the amorphous and graphitic, non-SWNT carbon species form at the early stages of carbon deposition rather than continuously during SWNT synthesis, possibly because they are formed on the more reducible cobalt. Similar results were previously reported by Alvarez et al. [15]. This behavior is consistent with large metallic particles being covered with graphitic carbon as soon as they are contacted with CO, while the SWNT growth initiated on Co clusters produced reduction of the cobalt ions from the pore walls on exposure to CO. Once they reach a critical size, these clusters initiate the growth of SWNT increasing the SWNT selectivity in the final product.

The diameter distribution of SWNT produced after catalyst exposure to CO for different durations was also characterized by NIR absorption spectroscopy, as shown in Fig. 10. The spectra recorded with catalyst samples exposed to CO for different durations are almost identical, indicating that the SWNT diameter distribution does not change significantly when the exposure to CO increased from 5 to 120 min, consistent with the conclusions drawn from the Raman results.

The carbon loading increased when the CO exposure increased from 5 to 30 min, as shown in the inset of Fig. 9. This behavior indicates that cobalt reduction and nucleation into metallic clusters and the CO disproportionation to grow carbon species are simultaneous and, thus, competitive processes. The carbon yield increases steeply during the first 30 min of CO exposure, and increases at a lower rate after subsequent exposure, consistent with previous results reported by Alvarez and co-workers [15]. However, the SWNT selectivity of the carbon grown at the early stages of CO exposure is lower compared to that of the carbon grown for longer time, as suggested by the weaker intensity of the RBM peak. This behavior suggests that cobalt reduction is faster at the early stages of CO exposure and some of the clusters nucleate into large particles selective for graphite deposition. The large particles are most likely formed from a small portion of the incorporated Co in the form of Co^{3+} ions that are not as strongly bound to the framework. Earlier studies showed a small portion of the incorporated Co (less than 4%) reduces at lower temperatures [39]. After the complete reduction of this Co^{3+} species, the Co reduction slows along with nucleation into clusters, and the SWNT growth rate exceeds the cluster growth rate. Thus the Co clusters have a higher probability of initiating SWNT growth (which stops cluster growth) before growing large enough to be nonselective for SWNT. Therefore, a slower rate of cobalt reduction is associated with a better SWNT selectivity.

Researchers have found that the growth rate of individual SWNT is very rapid, from a few milliseconds to about 1 s [4]. Alvarez and co-workers [16] have proposed that the yield of SWNT grown by CVD increases for hours [8,17,18]. This behavior has been attributed to a slow rate for the nucleation of metal particles. In these studies of SWNT growth on Co-Mo catalysts, the authors found that the carbon yield increased rapidly with reaction time during the first 2 h of CO exposure, while the SWNT selectivity remained relatively high. Our results obtained at different reaction times are consistent with these previously reported results.

Interestingly, unlike the strong effects of the prereduction and reaction temperatures, and of the CO pressure on the uniformity of SWNT diameter, the duration of catalyst exposure to CO does not seem to affect the diameter distribution of the SWNT. This behavior suggests that there is a rather narrow window of clusters sizes in which cobalt is selective for SWNT growth under high CO pressure and once that size is reached the SWNTs grow at a very fast rate and impede the further growth of the Co cluster initiating the growth of the nanotube.

The Co-MCM-41 catalysts loaded with carbon following exposure to CO for different durations were also investigated by X-ray absorption. Fig. 11 illustrates the near edge region of the spectra of Co-MCM-41 samples after exposure to 6 atm CO for different durations at 800 °C. While the intensity of the white line feature decreased and the intensity of the preedge peak increased as the duration of exposure of the catalyst to CO is increased from 5 to 15 to 30 min, the spectra recorded after catalyst exposure to CO for 60 and 120 min did not change significantly, suggesting that the cobalt clusters did not grow larger after 30 min exposure to CO. This has been confirmed by the evolution of the Co–Co and Co–O coordination numbers given in Table 2 as determined from the EXAFS spectra using the same procedure discussed above. The variation of Co–O coordination number with the

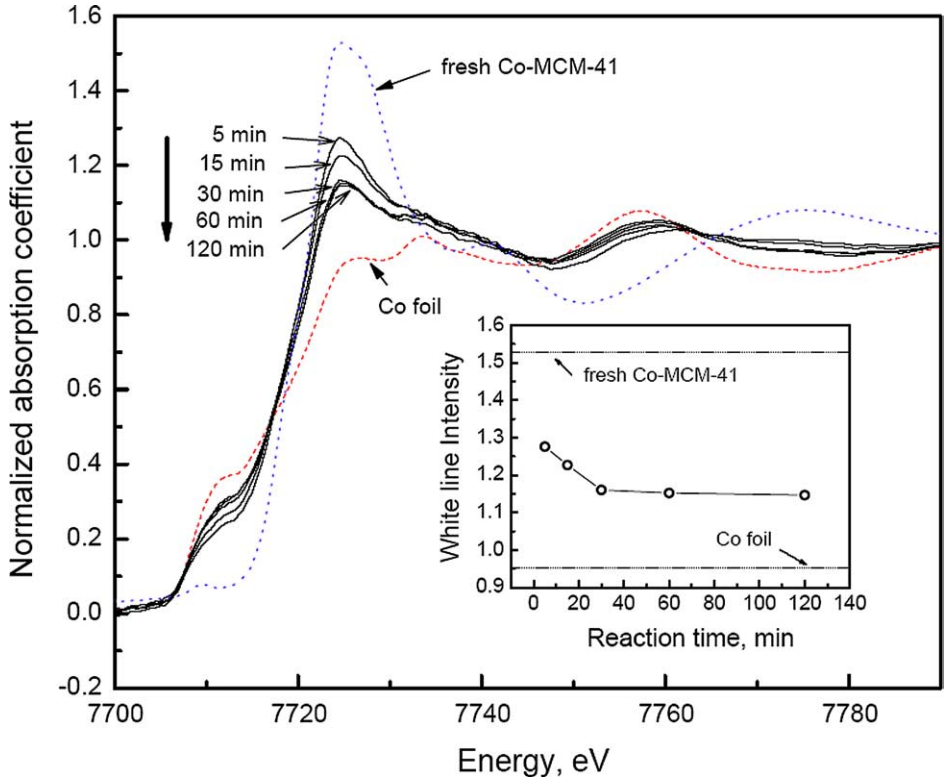

Fig. 11. Normalized EXFAS spectra near Co *K* edge recorded for Co-MCM-41 loaded with carbon at different reaction times. Spectra for the fresh Co-MCM-41 and cobalt foil are given as references. The inset shows the variation of the intensity of the white line with the reaction time.

Table 2
Structure parameters obtained from EXAFS fitting for Co-MCM-41 catalysts reacted for different durations

Reaction time (min)	Co–O first shell			Co–Co first shell		
	N_{Co-O} [a]	dR (Å) [b]	σ^2 [c]	N_{Co-Co} [d]	dR (Å) [b]	σ^2 [c]
5	1.18 ± 0.66	0.13 ± 0.02	1.05	4.43 ± 1.42	-0.03 ± 0.02	0.71
15	1.03 ± 0.47	0.13 ± 0.02	1.32	5.20 ± 1.25	-0.03 ± 0.01	0.74
30	0.78 ± 0.46	0.13 ± 0.02	1.26	6.81 ± 1.31	-0.02 ± 0.01	0.86
60	0.73 ± 0.27	0.13 ± 0.01	1.48	7.10 ± 0.87	-0.02 ± 0.01	0.80
120	0.71 ± 0.43	0.13 ± 0.03	1.29	7.13 ± 0.87	-0.03 ± 0.01	0.74

[a] N_{Co-O} average first-shell coordination of cobalt–oxygen.
[b] dR deviation from the effective half-path-length R (R is the interatomic distance for single scattering paths).
[c] σ^2 ($\times 10^{-2}$ Å^2) mean-square deviation in R.
[d] N_{Co-Co} average first-shell coordination of cobalt.

duration of CO exposure mirrors the changes in the intensity of the white line, showing the same plateau for CO exposures longer than 30 min.

4. Conclusion

For SWNT synthesis by CO disproportionation on Co-MCM-41 catalysts both selectivity to SWNT and their diameter uniformity depend on the relative rates of the following three competitive processes: reduction of cobalt, nucleation of the reduced cobalt atoms into clusters, and initiation and growth of the carbon nanotubes. The results presented here show that reaction at low CO pressures causes a slow rate of Co reduction, but also a slow rate of SWNT growth, allowing cobalt clusters to grow into larger sizes before they initiate the growth of SWNT, and leads to a wider distribution of SWNT diameters. In contrast, at high CO pressures, despite the higher Co reduction rates, the catalyst generates SWNT of uniform diameters likely because SWNT growth proceeds quickly once the catalyst cluster reaches the required size/conformation.

The experiments performed exposing the catalyst to CO for different durations indicated that this process variable significantly affects the SWNT synthesis performance only during the first 30 min of reaction. It has been shown that an initial amount of Co—likely the Co^{3+} species present in the fresh catalyst—is rapidly reduced and this process is associated with production of larger amounts of graphitic carbon. Exposure time to CO, however, does not significantly affect the diameter uniformity of the SWNT produced.

Acknowledgments

We thank DARPA-DSO for the financial support for this project. Partial support for the synthesis of the MCM-41 catalysts and the use of the National Synchrotron Light Source at Brookhaven National Laboratory were obtained from DoE-BES. We also thank Sang Nyon Kim and Pro-

fessor Fotios Papadimitrakopoulos at the University of Connecticut for support with the multiexcitation wavelength Raman characterization.

References

[1] T.W. Odom, J.-L. Huang, C.M. Lieber, Ann. N.Y. Acad. Sci. 960 (2002) 203.
[2] S. Lim, D. Ciuparu, C. Pak, F. Dobek, Y. Chen, D. Harding, L. Pfefferle, G. Haller, J. Phys. Chem. B 107 (2003) 11048.
[3] D. Ciuparu, Y. Chen, S. Lim, G.L. Haller, L. Pfefferle, J. Phys. Chem. B 108 (2004) 503.
[4] F. Kokai, K. Takahashi, M. Yudasaka, R. Yamada, T. Ichihashi, S. Iijima, J. Phys. Chem. B 103 (1999) 4346.
[5] E. Munoz, W.K. Maser, A.M. Benito, M.T. Martinez, G.F. de la Fuente, Y. Maniette, A. Righi, E. Anglaret, J.L. Sauvajol, Carbon 38 (2000) 1445.
[6] Y. Saito, Y. Tani, A. Kasuya, J. Phys. Chem. B 104 (2000) 2495.
[7] R. Zhang, R.K. Tsui, J. Tresek, A.M. Rawlett, I. Amlani, T. Hopson, P. Fejes, J. Phys. Chem. B 107 (2003) 3137.
[8] A.M. Cassell, J.A. Raymakers, J. Kong, H.J. Dai, J. Phys. Chem. B 103 (1999) 6484.
[9] W.Z. Li, J.G. Wen, Y. Tu, Z.F. Ren, Appl. Phys. A 73 (2001) 259.
[10] W. Liu, W. Cai, L. Yao, X. Li, Z. Yao, J. Mater. Sci. 38 (2003) 3051.
[11] M.J. Bronikowski, P.A. Willis, D.T. Colbert, K.A. Smith, R.E. Smalley, J. Vac. Sci. Technol. A 19 (2001) 1800.
[12] P. Nikolaev, M.J. Bronikowski, R.K. Bradley, F. Rohmund, D.T. Colbert, K.A. Smith, R.E. Smalley, Chem. Phys. Lett. 313 (1999) 91.
[13] C.E. Dateo, T. Gokcen, M. Meyyappan, J. Nanosci. Nanotechnol. 2 (2002) 523.
[14] T. Gokcen, C.E. Dateo, M. Meyyappan, J. Nanosci. Nanotechnol. 2 (2002) 535.
[15] W.E. Alvarez, B. Kitiyanan, A. Borgna, D.E. Resasco, Carbon 39 (2001) 547.
[16] W.E. Alvarez, F. Pompeo, J.E. Herrera, L. Balzano, D.E. Resasco, Chem. Mater. 14 (2002) 1853.
[17] M. Su, B. Zheng, J. Liu, Chem. Phys. Lett. 322 (2000) 321.
[18] J.H. Hafner, M.J. Bronikowski, B.R. Azamian, P. Nikolaev, A.G. Rinzler, D.T. Colbert, K.A. Smith, R.E. Smalley, Chem. Phys. Lett. 296 (1998) 195.
[19] H.J. Jeong, Y.M. Shin, S.Y. Jeong, Y.C. Choi, Y.S. Park, S.C. Lim, G.-S. Park, I.-T. Han, J.M. Kim, Y.H. Lee, Chem. Vapor Deposition 8 (2002) 11.
[20] O.A. Louchev, Y. Sato, H. Kanda, Appl. Phys. Lett. 80 (2002) 2752.
[21] Z.E. Horvath, L.P. Biro, G. Van Tendeloo, C. Tondeur, G. Bister, N. Pierard, A. Fonseca, J.B. Nagy, Diffus. Defect Data, Pt. B 94 (2003) 271.
[22] Y. Chen, D. Ciuparu, S. Lim, Y.Y., G.L. Haller, L. Pfefferle, J. Catal. 225 (2004) 453.
[23] A.M. Rao, E. Richter, S. Bandow, B. Chase, P.C. Eklund, K.A. Williams, S. Fang, K.R. Subbaswamy, M. Menon, A. Thess, R.E. Smalley, G. Dresselhaus, M.S. Dresselhaus, Science 292 (1997) 575.
[24] A.M. Rao, A. Jorio, M.A. Pimenta, M.S.S. Dantas, R. Saito, G. Dresselhaus, M.S. Dresselhaus, Phys. Rev. Lett. 84 (2000) 1820.
[25] M.S. Dresselhaus, A. Jorio, A.G. Souza, G. Dresselhaus, R. Saito, Phys. B 323 (2002) 15.
[26] R. Saito, A. Jorio, A.G. Souza, A. Grueneis, M.A. Pimenta, G. Dresselhaus, M.S. Dresselhaus, Phys. B 323 (2002) 100.
[27] M. Sugano, A. Kasuya, K. Tohji, Y. Saito, Y. Nishina, Chem. Phys. Lett. 292 (1998) 575.
[28] M.S. Dresselhaus, P.C. Eklund, Adv. Phys. 49 (2000) 705.
[29] M.S. Strano, C.A. Dyke, M.L. Usrey, P.W. Barone, M.J. Allen, H.W. Shan, C. Kittrell, R.H. Hauge, J.M. Tour, R.E. Smalley, Science 301 (2003) 1519.
[30] M.E. Itkis, D.E. Perea, S. Niyogi, S.M. Rickard, M.A. Hamon, B. Zhao, R.C. Haddon, Nano Lett. 3 (2003) 309.
[31] J.C. Charlier, P. Lambin, Phys. Rev. B 57 (1998) R15037.
[32] X. Liu, T. Pichler, M. Knupfer, M.S. Golden, J. Fink, H. Kataura, Y. Achiba, Phys. Rev. B 66 (2002) 045411.
[33] S.M. Bachilo, M.S. Strano, C. Kittrell, R.H. Hauge, R.E. Smalley, R.B. Weisman, Science 298 (2002) 2361.
[34] M.J. O'Connell, S.M. Bachilo, C.B. Huffman, V.C. Moore, M.S. Strano, E.H. Haroz, K.L. Rialon, P.J. Boul, W.H. Noon, C. Kittrell, J.P. Ma, R.H. Hauge, R.B. Weisman, R.E. Smalley, Science 297 (2002) 593.
[35] Y.F. Lian, Y. Maeda, T. Wakahara, T. Akasaka, S. Kazaoui, N. Minami, N. Choi, H. Tokumoto, J. Phys. Chem. B 107 (2003) 12082.
[36] R.B. Weisman, S.M. Bachilo, Nano Lett. 3 (2003) 1235.
[37] E.A. Stern, M. Newville, B. Ravel, Y. Yacoby, D. Haskel, Phys. B 209 (1995) 117.
[38] A.L. Ankudinov, B. Ravel, J.J. Rehr, S.D. Conradson, Phys. Rev. B 58 (1998) 7565.
[39] S. Lim, D. Ciuparu, Y. Chen, Y. Yang, L. Pfefferle, G.L. Haller, J. Phys. Chem. B (2004), in press.
[40] L. Campbell, L. Hedin, J.J. Rehr, W. Bardyszewski, Phys. Rev. B 65 (2002).
[41] R.B. Greegor, F.W. Lytle, J. Catal. 63 (1980) 476.
[42] G.H. Via, J.H. Sinfelt, F.W. Lytle, J. Chem. Phys. 71 (1979) 690.
[43] J. Moonen, J. Slot, L. Lefferts, D. Bazin, H. Dexpert, Phys. B 209 (1995) 689.
[44] D. Bazin, J.J. Rehr, J. Phys. Chem. B 107 (2003) 12398.
[45] J. Rostrup-Nielsen, D.L. Trimm, J. Catal. 48 (1977) 155.
[46] M.S. Tzou, H.J. Jiang, W.M.H. Sachtler, Appl. Catal. 20 (1986) 231.
[47] M.S. Tzou, B.K. Teo, W.M.H. Sachtler, Langmuir 2 (1986) 773.